The allosteric glycogen synthase kinase-3 inhibitor NP12 limits myocardial remodeling and promotes angiogenesis in an acute myocardial infarction model

Received for publication, August 25, 2017, and in revised form, October 19, 2017 Published, Papers in Press, October 25, 2017, DOI 10.1074/jbc.M117.814376

Jugajyoti Baruah[1], **Ryan Hitzman, Jane Zhang, Suhnrita Chaudhuri**[2], **Victoria Mastej**[3], **and Kishore K. Wary**[4]
From the Department of Pharmacology, University of Illinois, Chicago, Illinois 60612

Edited by Roger J. Colbran

A key feature of acute myocardial infarction (AMI) is an alteration in cardiac architecture. Signaling events that result in the inhibition of glycogen synthase kinase-3 (GSK-3)β represent an adaptive response that might limit the extent of adverse remodeling in the aftermath of AMI. Here, we report that an allosteric inhibitor of GSK-3β, 4-benzyl-2-(naphthalene-1-yl)-1,2,4-thiadiazolidine-3,5-dione (NP12), lessens the magnitude of adverse myocardial remodeling and promotes angiogenesis. Male and female mice 8–10 weeks old were grouped (six animals in each group) into sham surgery (sham group), left anterior descending (LAD) ligation of the coronary artery followed by intramyocardial PBS injections (control group), and LAD ligation followed by NP12 administration (NP12 group). After 7 and 14 days, the extents of fibrosis and integrity of blood vessels were determined. Intramyocardial administration of NP12 increased phosphorylation of GSK-3β, reduced fibrosis, and restored diastolic function in the mice that had experienced an AMI. Morphometric analyses revealed increased $CD31^+$ and $Ki67^+$ vascular structures and decreased apoptosis in these mice. NP12 administration mediated proliferation of reparative cells in the AMI hearts. In a time-course analysis, Wnt3a and NP12 stabilized β-catenin and increased expression of both Nanog and VEGFR2. Moreover, NP12 increased the expression of β-catenin and Nanog in myocardium from AMI mice. Finally, loss- and gain-of-function experiments indicated that the NP12-mediated benefit is, in part, Nanog-specific. These findings indicate that NP12 reduces fibrosis, reestablishes coronary blood flow, and improves ventricular function following an AMI. We conclude that NP12 might be useful for limiting ventricular remodeling after an AMI.

One of the key features of acute myocardial infarction (AMI)[5] includes alterations of cardiac architecture, and the clearest pathology is the development of fibrotic lesion (1). Structural alterations seen after AMI are not restricted to the infarcted area but may also include the non-infarcted region of the heart (1, 2). Pathological changes in the non-infarcted heart include hypertrophy of the cardiomyocytes, neovascularization, and fibrosis. The fibrotic lesion found in the peri-infarct and in the non-infarct heart area leads to chamber dysfunction and increased ventricular stiffness thereby reducing cardiac compliance. However, reestablishing blood supply is a key determinant of cardiac function after AMI (3–5). In the aftermath of AMI, both short- and long-term, signaling mechanisms are activated to limit the extent of myocardial damage and to reduce fibrosis, and these preventive mechanisms can be collectively referred to as adaptive response (4–7). Animal experiments and genetic studies show that this adaptive response is associated with the inhibition of glycogen synthase kinase-3β (GSK-3β) (6–10). GSK-3β is a multifunctional serine/threonine kinase protein (7–9). Increased phosphorylation of GSK-3β (Ser-9) and thereby the inhibition of GSK-3β results in the inhibition or delayed opening of the mitochondrial permeability transition pore in cardiomyocytes, a *bona fide* regulator of apoptosis (8–14). However, increased phosphorylation of GSK-3β (Ser-9) also results in the stabilization of β-catenin, and stabilized β-catenin species accumulate in the nucleus to convert the T-cell factor (TCF)4/lymphoid-enhancer factor (LEF)1 repressor complex into a transcriptional activator complex to stimulate canonical Wnt signaling (15–18). Activation of canonical Wnt signaling increases expression of Nanog in endothelial cells (ECs) (19, 20). These observations raise an important question of whether the allosteric inhibition of GSK-3β might reduce the extent of adverse myocardial remodeling seen after AMI, and whether increased Nanog expression might be associated with restoration of coronary blood supply.

The recently described 4-benzyl-2-(naphthalene-1-yl)-1,2,4-thiadiazolidine-3,5-dione, also known as NP12, is a small-molecule allosteric inhibitor of GSK-3β (21). NP12 was

This work was supported in part by the National Institutes of Health Grant HL079356, American Heart Association Grants GRNT25710129 and GRNT33700162, and by University of Illinois at Chicago Center for Clinical and Translation Science Award UL1RR029879 (to K. K. W.). The authors declare that they have no conflicts of interest with the contents of this article. The content is solely the responsibility of the authors and does not necessarily represent the official views of the National Institutes of Health.
This article contains supplemental Figs. S1–S13.
[1] Supported by American Heart Association Pre-doctoral Fellowships (Mid-West affiliate) 15PRE22760004 and CCTS-PECTs 1UL1TR002003.
[2] Supported by the Fulbright-Nehru Fellowship Program (2038/FNPDR/2015).
[3] Supported by CCTS-PECTs Grant 1UL1TR002003.
[4] To whom correspondence should be addressed: Dept. of Pharmacology, University of Illinois, 835 S. Wolcott Ave., Rm. E403, Chicago, IL 60612. Tel.: 312-413-9582; Fax: 312-996-1225; E-mail: kkwary@uic.edu.

[5] The abbreviations used are: used: AMI, acute myocardial infarction; ANOVA, analysis of variance; EC, endothelial cell; HPAEC, human pulmonary arterial endothelial cell; HUVEC, human umbilical vein endothelial cell; HSaVEC, human saphenous-vein EC; WB, Western blotting; LAD, left anterior descending; vWF, von Willebrand factor; UIC, University of Illinois at Chicago; PI, propidium iodide; EF, ejection fraction; FS, fractional shortening; LV, left ventricular; APC, allophyocyanin.

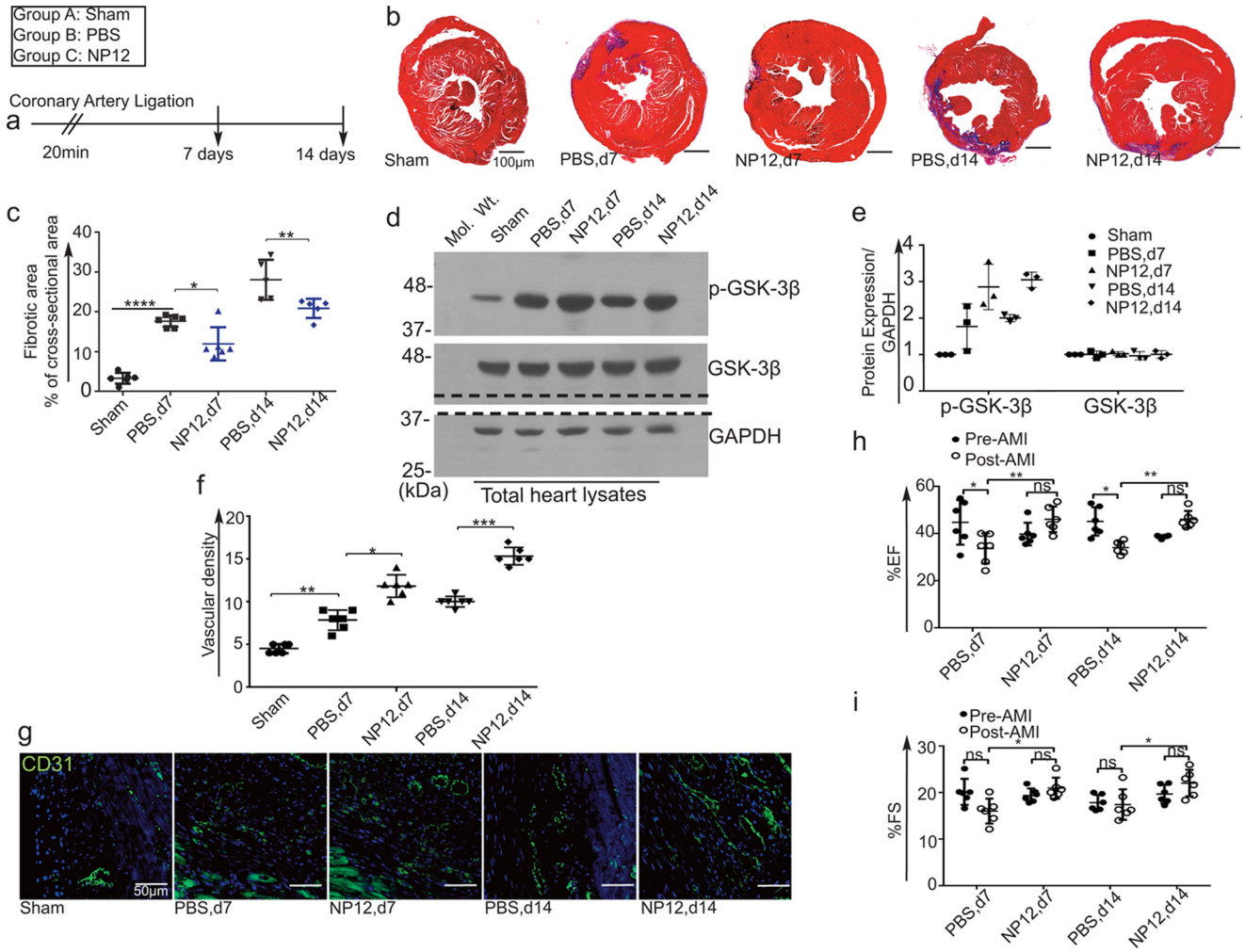

Figure 1. Allosteric inhibition of GSK-3β limits the extent of myocardial fibrosis and restores coronary blood vessels in a mouse model of AMI. *a,* timeline of experiment. *b,* representative trichrome staining of animal cohorts: sham (+NP12, $n = 6$ animals each group/time point); hearts receiving PBS ($n = 6$ animals each group/time point); and NP12 ($n = 6$ animals each group/time point) at day 7 post-AMI; infarcted hearts receiving PBS ($n = 6$ animals each group/time point) and NP12 ($n = 6$ animals each group/time point) 14 days post-AMI. *c,* quantification of fibrotic area in sham and infarcted hearts receiving PBS or NP12 at days 7 and 14; data were subjected to ANOVA followed by Sidak's test. *d,* levels of p-GSK-3β(Ser-9), total GSK-3β in the sham and in infarcted hearts. The *dotted line* indicates the position where the nitrocellulose membrane was cut. *e,* quantification of signal intensities of WBs shown in *d*; each data point represents mean value calculated from two mice ($n = 6$ mice per group). *f,* quantification of $CD31^+$ vascular structures at days 7 and 14 in the infarcted zones as compared with the PBS group; each data point represents mean value calculated from five microscopic fields/mice that were selected from the infarcted area ($n = 6$ mice per group). *g,* representative fluorescent images (×20) of $CD31^+$ (*green*) in the infarcted myocardium at days 7 and 14, receiving either PBS (vehicle) or NP12 *versus* controls. *h* and *i,* ejection fraction (*EF%*) and fractional shortening (*FS*) in mouse hearts receiving NP12 at days 7 and 14, $n = 6$ mice per group; data were subjected to ANOVA followed by Tukey's test. *Error bars* represent ± S.D. *, $p < 0.05$; **, $p < 0.01$; ***, $p < 0.001$; ****, $p < 0.0001$ *versus* PBS (vehicle) group or *versus* pre-AMI. *Scale bars* are as shown. Abbreviations: *d7,* day 7; *d14,* day 14; *ns,* not significant.

explored as a potential treatment for Alzheimer's disease and supranuclear palsy in phase-IIa and -IIb clinical trials (21, 22). In animal experiments, administrations of NP12, including intravenous route, reduced cerebral atrophy and provided anti-inflammatory benefits with no apparent toxicity (21–25). Because fibrosis and reduced perfusion are the main causes of pathological remodeling after AMI, here we tested the hypothesis that NP12 might limit the extent of myocardial remodeling and restore coronary blood supply.

Results

Intramyocardial administration of NP12 limits the extent of adverse remodeling and restores coronary blood supply in the aftermath of AMI

To test the efficacy of allosteric inhibition of GSK-3β by NP12, we subjected wild-type C57BL/6N mice to left anterior descending (LAD) ligation of the coronary artery for 20 min to induce AMI. A ligation period of 30 min or less restored the ECG to baseline, without causing permanent changes to the ECG, reducing mortality and minimizing the phenotypic complexity seen after the AMI. We chose a 20-min transient LAD ligation of the coronary artery, whereby the QT-interval widened and the ST-segment remained elevated (26–28), indicating an ongoing ischemic event to the myocardium. Thus, we designed experiments to create myocardial infarction following a 20-min ligation of the LAD coronary artery (Fig. 1*a*). Although NP12 can be administered intravenously, however, our goal was to study the effect of NP12 on local cardiac remodeling; therefore, the intramyocardial administration method allowed us to use an optimal and effective concentration of NP12 (29). In pilot experiments, sham operated mice did not show any appreciable changes in cardiac parameters

(supplemental Fig. S1). In NP12-treated mice, we observed increased Akt phosphorylation, indicating activation of the survival pathway (supplemental Fig. S2). Masson's trichrome staining of sham, and AMI hearts receiving vehicle alone (−NP12) or GSK-3β inhibitor (+NP12) at days 7 and 14 post-AMI revealed the degree of myocardial fibrosis. Mice receiving NP12 showed a significant reduction (*, $p < 0.05$, and **, $p < 0.01$ *versus* PBS) in fibrotic scarring as compared with increased scarring observed in mice receiving PBS (Fig. 1, *b* and *c*, and supplemental Fig. S3). In our experiments, the use of isoflurane (30, 31) and etomidate in the PBS (vehicle) receiving myocardium did not show an appreciable decrease in infarct size (Fig. 1, *b* and *c*, and supplemental Fig. S3) or improvement of cardiac functions (Fig. 1, *h* and *i*). In addition, we also analyzed expression levels of phospho- and total GSK-3β in heart lysates of sham-, vehicle-, and NP12-receiving groups. Accordingly, we found an increased expression of p-GSK-3β in NP12-receiving groups at days 7 and 14 (Fig. 1, *d* and *e*).

Re-establishing blood flow after AMI reduces the extent of myocardial remodeling and improves cardiac function (32, 33). To assess the extent of coronary vascularization in response to NP12, vascular density in the infarcted and border zones was measured by staining with anti-$CD31^+$ antibody (Fig. 1, *f* and *g*). Mice receiving PBS showed an appreciable increase in capillaries and capillary-like vascular structures, whereas NP12 treatment significantly increased (*, $p < 0.05$ *versus* PBS day 7 and ***, $p < 0.001$ *versus* PBS, day 14) microvessel-like structures in and around the infarcted area. AMI initiates progressive left ventricular (LV) remodeling, leading to deterioration of cardiac function. To evaluate functional recovery in response to NP12 treatment, we compared ECGs from pre-AMI and post-AMI mice at days 7 and 14. In line with previous observations, mice receiving NP12 showed significant improvements in cardiac parameters associated with the ejection fraction (EF%, **, $p < 0.01$ *versus* PBS) and fractional shortening (FS%, *, $p < 0.05$ *versus* PBS), indicating a recovery of LV function (Fig. 1, *h* and *i*). In addition, there was a significant reduction in diastolic parameters, including isovolumetric relaxation time and the E wave deceleration time (supplemental Fig. S4) in PBS groups compared with the NP12 receiving groups, indicating a decline in cardiac function. These findings suggest that NP12 administration reduced fibrosis, mediated angiogenesis, and improved cardiac function in these mice.

NP12 mediates increased proliferation and survival of ECs

ECs play key roles in post-AMI-related revascularization and reperfusion, facilitating efficient myocardial repair (34–36). Because we observed robust revascularization in infarcted hearts receiving NP12, we next tested the capacity of administration of NP12 to mediate angiogenic activities of ECs. We first optimized NP12 dosage using ECs (supplemental Fig. S5*a*) in the presence of $VEGF^{165}$ (5 ng/ml) and serum to elicit a cell-proliferative response. We also used flow cytometry to assess whether there was an increase in cell survival (supplemental Fig. S5*b*), subsequently determining that a dose of 60 nmol/liter NP12 was optimal for future *in vitro* and *ex vivo* assays.

To evaluate NP12-mediated EC proliferation, we measured BrdU incorporation as an indicator of cells entering the S-phase of the cell cycle in HUVECs, HSaVECs, and HPAECs. The timeline of the experiment is presented in Fig. 2*a*. In the absence of VEGF and NP12, cells exhibited basal levels of proliferation, whereas the proportion of cells receiving both VEGF and NP12 exhibited a significant (**, $p < 0.01$ *versus* VEGF only, ****, $p < 0.0001$ *versus* control) number of proliferating cells *versus* cells receiving VEGF or NP12 alone (Fig. 2*c* and supplemental Fig. S6, *a–d*).

Next, we examined whether the increase in EC proliferation was accompanied by an increase in cell survival. The timeline for the apoptosis assay is shown in Fig. 2*b*. Accordingly, ECs were serum-deprived overnight; thereafter, the EC basal media were supplemented with a combination of VEGF, NP12, or both. Cells receiving VEGF and NP12 exhibited a significantly lower population of cells positive for annexin-V and propidium iodide (PI) staining (Fig. 2*d*). These results indicated that NP12 administration, in combination with VEGF, protected cell death, thereby favoring a survival phenotype in ECs.

Furthermore, we addressed whether NP12 administration could stimulate proliferation and survival of reparative cells. Accordingly, heart sections prepared from these mice were evaluated by co-staining with Ki67 (a cell-proliferation marker) and vWF (an EC marker) and by TUNEL staining (Fig. 2, *e–h*, and supplemental Figs. S7 and S8). The number of cells expressing Ki67 was significantly higher (*, $p < 0.05$ *versus* PBS, d7; ***, $p < 0.001$ *versus* PBS, d14) in the group receiving NP12 as compared with that observed in the group receiving PBS (Fig. 2*e*). Moreover, TUNEL staining indicated a significant reduction (***, $p < 0.001$ *versus* PBS, d7) in apoptotic nuclei in the NP12-receiving group (Fig. 2*f*). In addition, NP12 administration reduced cell death in EC and non-EC populations in the infarcted myocardium, as illustrated by the microscopic analyses of myocardial sections with anti-annexin-V, an apoptotic marker, and anti-CD31 (supplemental Fig. S8)

NP12 mediates angiogenic phenotypes of ECs

To address whether NP12 mediates repair and reestablishment of coronary blood vessels, we performed *in vitro* wound healing and Boyden chamber transfilter assays (Fig. 3*a*). Scratches introduced in a monolayer of ECs that received either vehicle PBS alone (−NP12) or 60 nmol/liter NP12 were photographed at 3 and 6 h. Quantification of the area covered by migrating ECs indicated that NP12 treatment resulted in a significant rate (**, $p < 0.01$ *versus* 3 h, ***, $p < 0.001$ *versus* 6 h) of wound closure at 6 h as compared with that observed in the control group (Fig. 3, *b* and *c*). This was validated by our observation of an increased chemotactic migration of ECs across transfilters toward NP12-containing wells (Fig. 3, *d* and *e*).

In addition to proliferation and migration, ECs sprouting and tube formation are necessary for re-establishing blood supply. The aortic ring microvessel sprouting assay mimics the different phases of aortic angiogenesis. Fig. 3, *f* and *g*, shows the ability of NP12 to augment microvessel outgrowth from the aortic rings. Together, these results indicated that NP12 administration enhanced the angiogenic phenotype of ECs to reestablish coronary blood supply as seen in NP12-treated AMI hearts.

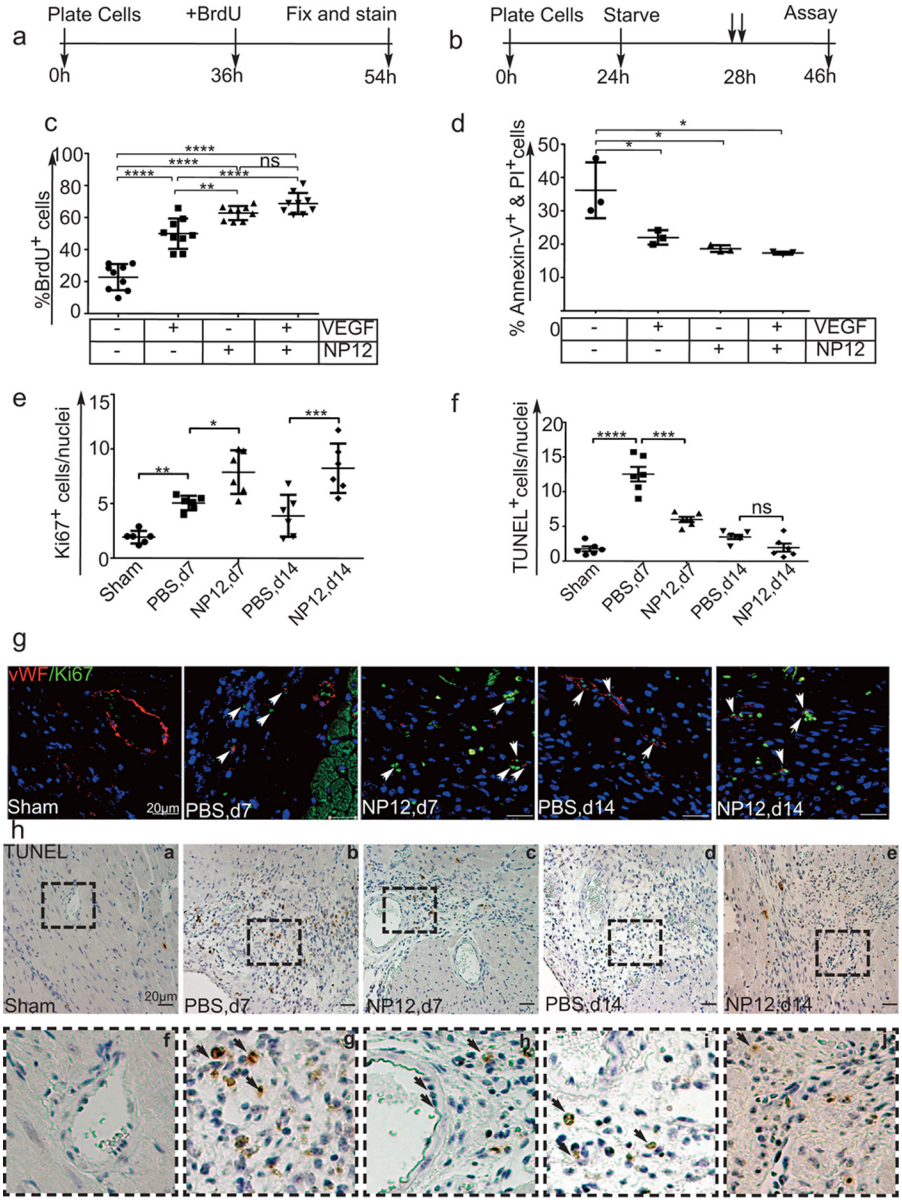

Figure 2. NP12-mediated allosteric inhibition of GSK-3β induces proliferation and survival of ECs. *a,* timeline of the BrdU incorporation assay. *b,* timeline of the apoptosis assay. *c,* ECs in 24-well plates were treated for 18 h with either 60 nmol/liter NP12, VEGF (5 ng/ml), or both in the presence of BrdU. The $BrdU^+$ and $BrdU^-$ cells were counted, and thereafter the percentage of BrdU-positive cells was calculated. Administration of NP12 alone or in combination with VEGF significantly increased the number of proliferating ECs (****, $p < 0.0001$) *versus* untreated controls; where each data point represents the mean calculated from three technical replicates, and data were subjected to ANOVA followed by Sidak's test. *d,* ECs were serum-starved for 4 h. To minimize cell death, we included insulin, transferrin, and selenium (1× ITS) in basal media during the 4-h starvation period. Subsequently, media supplemented with VEGF (5 ng/ml) or NP12 (60 nmol/liter), or both, were added prior to 18 h of incubation. ECs labeled with annexin-V–APC and PI were subjected to FACS analysis. Percentages of annexin-V-positive and PI-positive cells were decreased in VEGF and NP12-treated populations; each data point represents an independent experiment performed with two technical replicates, and thereafter the data were subjected to ANOVA followed by Sidak's test. *e* and *f,* quantification of $Ki67^+$ and $TUNEL^+$ cells in NP12-receiving myocardial sections at days (*d*) 7 and 14 *versus* PBS-receiving group was subjected to ANOVA followed by Sidak's test. *g,* representative images of $Ki67^+$ (×63, *green*) and vWF^+ (*red*) structures indicated by *white arrows* in the infarcted myocardium at days 7 and 14, receiving either PBS or NP12. *h, top panels, a–e,* representative $TUNEL^+$ (×20, *brown*) structures in the infarcted myocardium at days 7 and 14, receiving either PBS or NP12. *Bottom panels, f–j,* represent magnified images (*inset*), and *black arrows* indicate the endothelium. *Error bars* represent ± S.D. *, $p < 0.05$; **, $p < 0.01$; ***, $p < 0.001$; ****, $p < 0.0001$ *versus* indicated groups ($n = 6$ animals each group per time point). *Scale bars* are as shown. Abbreviations: *VEGF,* vascular endothelial growth factor; *APC,* allophyocyanin; *TUNEL,* terminal deoxynucleotidyltransferase dUTP nick end labeling. *ns,* not significant.

NP12 mediates robust activation of the Wnt-signaling pathway

To elucidate the mechanism of apparent benefit observed in our AMI model, we determined the transcriptional target of NP12 in ECs. Because GSK-3β is an important regulatory kinase in the canonical Wnt-signaling pathway, we tested whether this novel allosteric inhibitor of GSK-3β could modulate Wnt signaling. Accordingly, ECs and HEK293 cells were transfected with the Wnt reporter TOPFlash plasmid construct-harboring promoter with eight copies of TCF4-binding sites (Fig. 4*a*). We observed increased TCF4 promoter-driven luciferase activity in response to Wnt3a and NP12 (Fig. 4*b* and supplemental Fig. S9). To verify that this increase in luciferase activity was due to β-catenin translocation into the nucleus, we

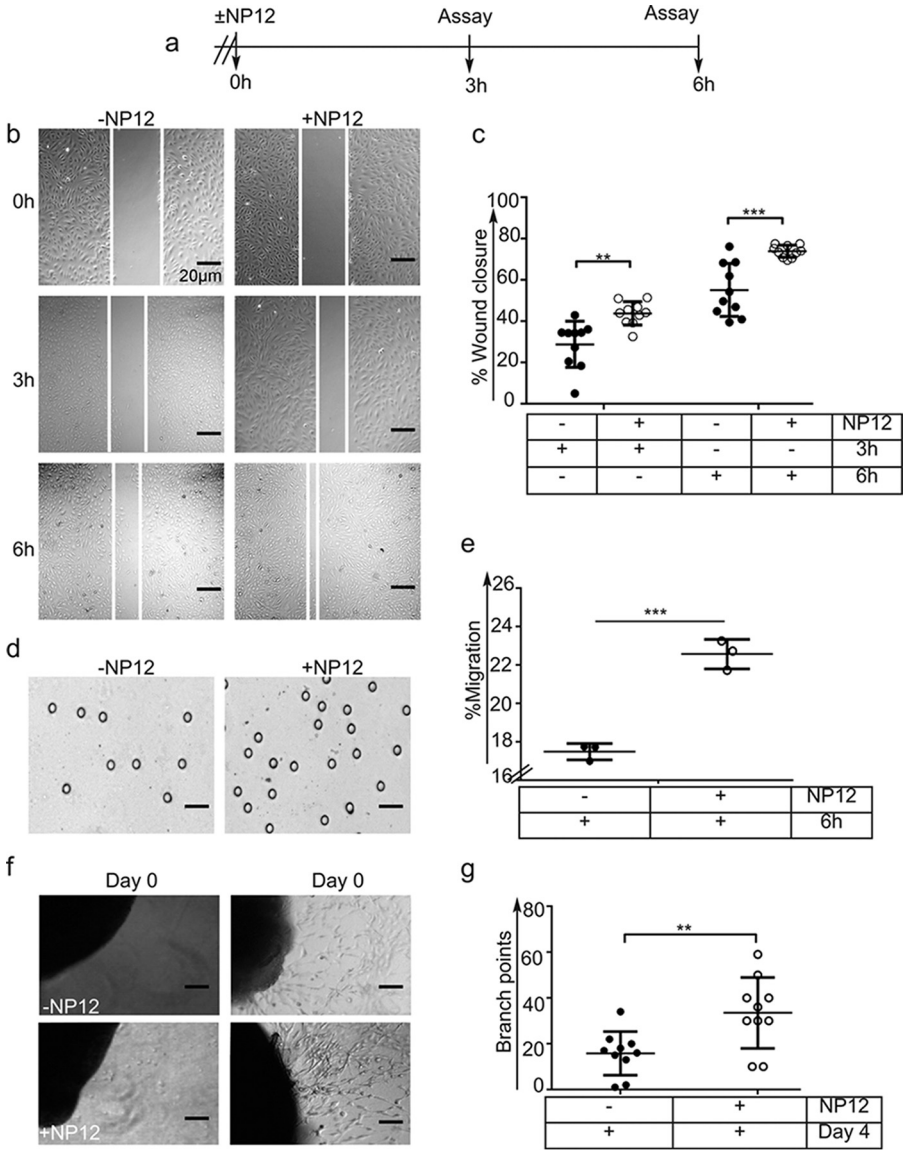

Figure 3. Inhibition of GSK-3β mediates EC migration and sprouting of aortic ring. *a,* timeline for the wound closure assay. A sterile 200-μl pipette tip was used to introduce a physical wound (scratch); thereafter, complete media (control) or media with NP12 (60 nmol/liter) were added to the wells. Representative images of NP12-treated ECs with wound closure at the indicated time points are shown (×10). *b* and *c,* extent of wound closure (in percentage) was calculated at 3 and 6 h. **, $p < 0.01$ *versus* 3-h control; ***, $p < 0.001$ *versus* 6-h control, where each data point represents an independent experiment performed with two technical replicates and thereafter was subjected to ANOVA followed by Sidak's test. *d,* to investigate chemotactic migration of ECs toward NP12-containing wells, ECs were seeded on the top chamber and separated by a porous membrane. The lower chambers were filled with media (vehicle) or media with NP12 (60 nmol/liter). After 6 h, cells that migrated across the membrane were fixed and counted. Representative images of EC migration are in response to NP12. Magnifications are as shown. *e,* quantification revealed increased migration of ECs in response to NP12. ***, $p < 0.001$ *versus* control; each data point represents an independent experiment, where each experiment was conducted with three technical replicates; thereafter, the data were analyzed by unpaired *t* test. *f,* aortic rings were embedded in a fibrin matrix, and thereafter EC media (vehicle) or NP12 (60 nmol/liter) was added. Microvessel ECs sprouting from aortic explants were imaged on consecutive days, and media were replenished every 48 h. *g,* quantification of branching point structures, **, $p < 0.01$ *versus* control was analyzed by unpaired *t* test; $n = 10$ aortic rings per conditions. Magnifications are as shown. *Error bars* represent ± S.D.

performed cell fractionation analysis. Nuclear and cytoplasmic fraction from control and NP12-treated ECs were prepared and analyzed by WB. As expected, the nuclear fraction of NP12-treated ECs showed increased accumulation of β-catenin, whereas the cytoplasmic fraction showed increased cyclin-D1. The purity of fractions was confirmed by probing the membrane with the cytoplasmic loading control, GAPDH, and the nuclear loading control, Lamin-B1 (Fig. 4*c*). Microscopic analysis also confirmed that ECs stained with anti-β-catenin and VE-cadherin showed increased accumulation of nuclear β-catenin as compared with levels observed in control cells (Fig. 4, *d* and *e*). Additionally, high resolution confocal *z*-stack imaging showed co-localization of β-catenin and TCF4 in the nucleus of NP12-treated ECs (Fig. 4*f* and supplemental Fig. S10). These results indicated that NP12 administration mediated strong activation of canonical Wnt signaling in ECs.

NP12 induces the expression of Nanog and cyclin-D1

Next, we determined the ability of NP12 to mediate the activation of Wnt signaling in ECs. Accordingly, in ECs treated with 60 nmol/liter NP12, the expression of β-catenin and Nanog increased in a time-dependent manner, with

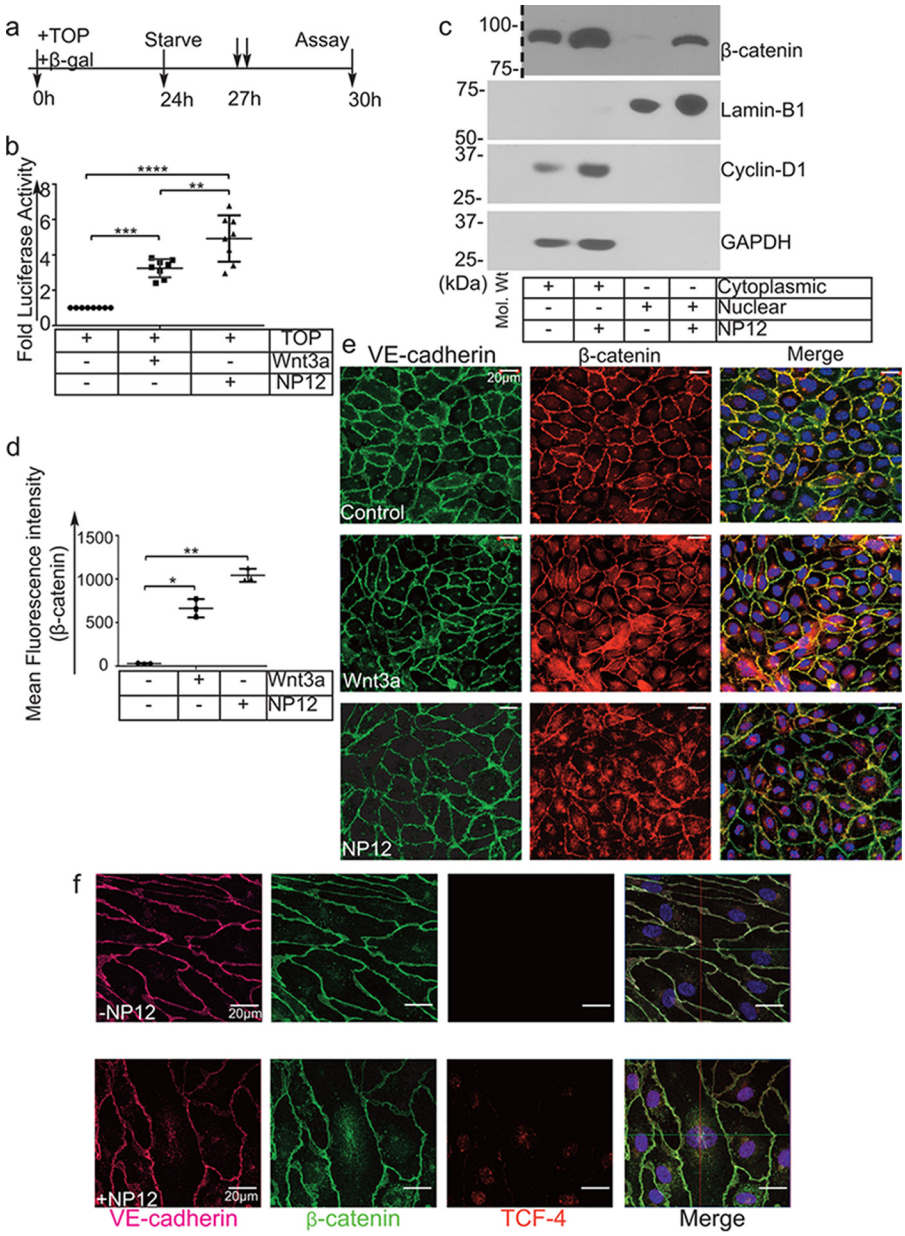

Figure 4. Allosteric inhibition of GSK-3β mimics canonical Wnt signaling. *a,* timeline of the TOPFlash luciferase assay. *b,* ECs were transiently transfected with the TOPFlash plasmid and reporter β-gal and thereafter treated with (↓ ↓) Wnt3a or NP12 for 3 h. The *TCF4*-promoter luciferase activity following NP12 treatment is presented as fold luciferase activity; experiments were performed four times with two technical replicates, and each data point represents one technical sample; thereafter, data were subjected to ANOVA followed by Sidak's test. *c,* cytoplasmic and nuclear fractions prepared from control ECs or ECs receiving NP12 (60 nmol/liter for 6 h) were analyzed by immunoblotting with β-catenin and cyclin-D1 antibodies. *Dotted line* indicates the position where the nitrocellulose membrane was cut. The cytoplasmic and nuclear fractions prepared from NP12-treated ECs showed increased accumulation of β-catenin in both compartments, whereas cyclin-D1 was primarily detected in the cytoplasmic fraction. For loading controls, we used GAPDH and lamin-B1. *d* and *e,* control ECs (vehicle) or ECs receiving NP12 (60 nmol/liter) were fixed and stained with anti-VE-cadherin (*green*) and anti-β-catenin (*red*). Control ECs showed β-catenin (*red*) largely at the membrane; in contrast, NP12-treated ECs showed increased cytoplasmic, some perinuclear, and nuclear staining (×40). Each data point represents the mean value, and each experiment was performed with three technical replicates; thereafter, data were subjected to ANOVA followed by Dunnett's test. *f,* high-resolution (×63) confocal *z*-stack imaging showed co-localization of β-catenin (*green*) with TCF4 (*red*) in the nucleus of NP12-treated ECs as compared with that observed in controls. VE-cadherin (*magenta*). *Error bars* represent ± S.D. *, $p < 0.05$; **, $p < 0.01$; ***, $p < 0.001$; ****, $p < 0.0001$ *versus* indicated groups. *Scale bars* are as shown.

maximal expression observed as early as 3 h post-treatment (Fig. 5, *a* and *b*). We also observed an increased phosphorylation of GSK-3β (Ser-9) (Fig. 5*c*). Next, we assessed the expression of Wnt target genes cyclin-D1 and *VEGFR2* (Fig. 5*d*). Compared with untreated ECs, the expression of cyclin-D1 increased after 40 min post-treatment, whereas *VEFGR2* expression oscillated. Wnt3a, the natural ligand that activates canonical Wnt signaling, was used as a positive control. Given that the ECs were not starved of growth factors or serum for this experiment, we observed basal levels of β-catenin, Nanog, and VEGFR2 protein expression in the lysates. Furthermore, immunostaining of NP12-treated ECs showed increased nuclear staining for Nanog (Fig. 5*e*). These results indicated that treatment with nanomolar concentrations of NP12 was sufficient to modulate Wnt signaling in ECs.

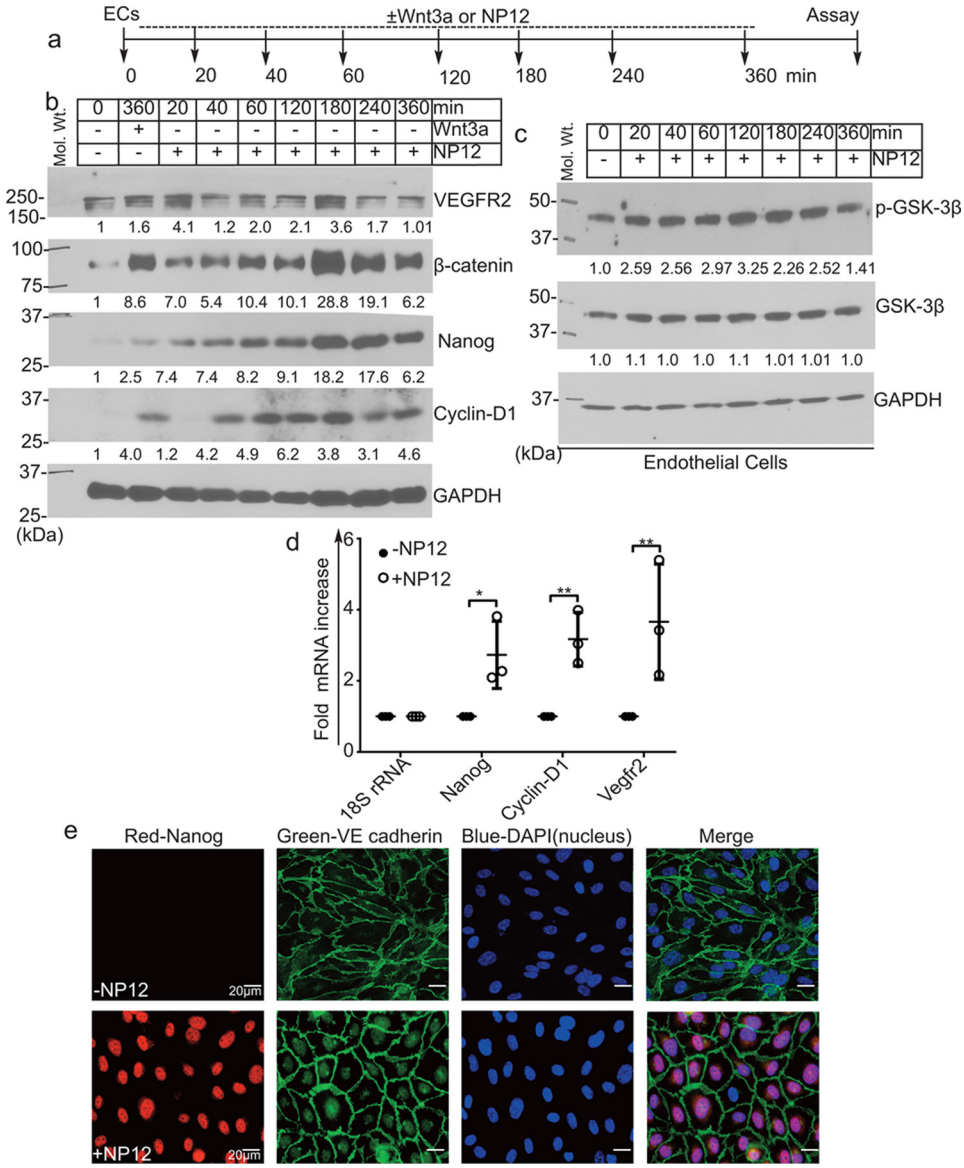

Figure 5. Inhibition of GSK-3β promotes robust expression of Nanog and cyclin-D1 in ECs. *a,* timeline of experiment. ECs in culture were treated with either Wnt3a (50 ng/ml) alone for 360 min or NP12 (60 nmol/liter) for 0, 20, 40, 60, 120, 180, 240, and 360 min. *b,* NP12 increased stabilization of β-catenin in a time-dependent manner. EC extracts were analyzed by immunoblotting with anti-β-catenin antibody that detects total β-catenin. Accumulation of β-catenin can be detected as early as 20 min post-treatment, as well as robust accumulation by 3 h, as compared with results observed in Wnt3a-stimulated cells, which showed significant but lower levels of induction after 6 h. WB analyses showed increased expression of Wnt target proteins in a time-dependent manner following NP12 treatment. For loading control, we used anti-GAPDH. *c,* EC lysates prepared from NP12-treated cells were analyzed with anti-p-GSK-3β, anti-GSK-3β, and anti-GAPDH antibodies. *d,* q-RT-PCR analysis indicated increased levels of *Nanog,* cyclin-D1, and *VEGFR2* transcripts in ECs following NP12 treatment. Each data point represents mean value from an independent experiment; each experiment was conducted with three technical replicates; thereafter, data were subjected to ANOVA followed by Sidak's test. *e,* microscopic analyses of control ECs and ECs receiving NP12 (60 nmol/liter) with anti-Nanog (*red*) and anti-VE-cadherin (*green*) showed robust increases in nuclearly-localized Nanog. The *numbers* at the *bottom* of the panels indicate fold intensity. *, $p < 0.05$; **, $p < 0.01$ *versus* indicated groups. Experiments were performed with six mice in each group ($n = 6$), and *in vitro* data were obtained from three independent experiments. *Error bars* represent ± S.D. *Scale bars* are as shown. Abbreviation: *VEGFR2,* vascular endothelial growth factor receptor 2.

Nanog is highly enriched in CD31$^+$ vascular structures in myocardial tissues receiving NP12

Next, we validated the expression of Nanog in the infarcted hearts. To localize and identify β-catenin$^+$, Nanog$^+$, and ECs (CD31$^+$) cells *in vivo*, groups of mice were subjected to AMI, treated with PBS or NP12, and thereafter heart tissues were collected at day-7 and -14 time points. Microscopic examination of these sections indicated the presence of an increased expression of Nanog and β-catenin proteins in CD31$^+$ ECs (Fig. 6, *a* and *b*). Next, mRNAs prepared from CD31$^+$ cardiac ECs confirmed the increased expression of *Nanog*, as well as cyclin-D1, *Ki67,* and *VEGFR2* in these cells (Fig. 6, *c–f*). WB analysis also confirmed the increased expression of p-GSK-3β, VEGFR2, β-catenin, and Nanog proteins in hearts that received NP12, compared with PBS (supplemental Figs. S11 and S12). These results further confirmed our *in vitro* observation that the allosteric inhibitor of GSK-3β stabilizes β-catenin and up-regulates Nanog expression. Mouse fibroblast cells did not express endogenous Nanog; importantly, NP12 did not induce the expres-

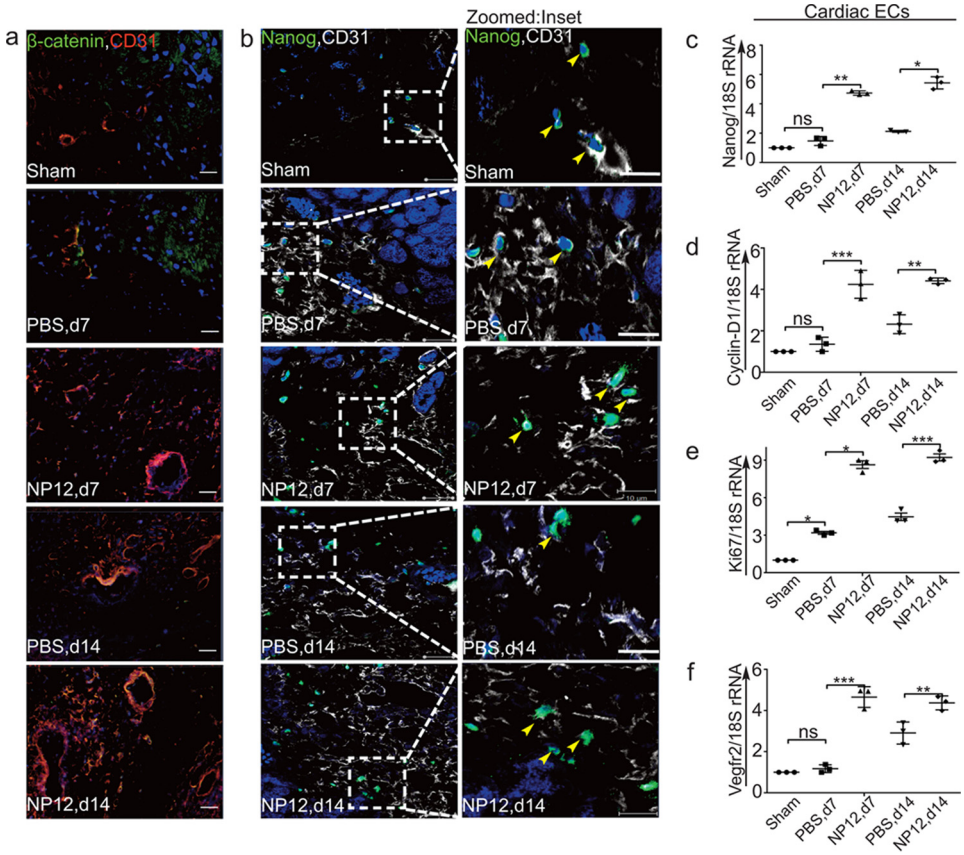

Figure 6. NP12 mediates up-regulation of Nanog in infarcted myocardium. *a,* representative immunofluorescence analysis of β-catenin (*green*) and CD31 (*red*) double-labeling in the infarcted myocardium at days (*d*) 7 and 14, receiving either PBS or NP12 *versus* sham. *b,* representative confocal images of double-staining with Nanog (*green*) with CD31 (for optimal resolution, the *red color* is converted into *white*) in the infarcted myocardium at days 7 and 14, receiving either PBS or NP12 *versus* sham heart. *Panels* to the *right* of *b* show magnified images with *yellow arrowheads* indicating co-localization of nuclear Nanog with $CD31^+$ vascular structures. *c–f,* mRNAs prepared from $CD31^+$ cardiac ECs obtained from sham-, PBS-, and NP12-receiving mice were analyzed by qRT-PCR for expression of *Nanog,* cyclin-D1, *Ki67,* and *Vegfr2* transcripts using 18S rRNA as internal control. Data show a significant increase in expression of target genes compared with the indicated groups; thereafter, data were subjected to ANOVA followed by Sidak's test. We used $n = 3$ mice each group for qRT-PCR analysis, and $n = 6$ mice each group for immunostaining. *Error bars* represent ± S.D. *, $p < 0.05$; **, $p < 0.01$; ***, $p < 0.001$ *versus* indicated groups. *ns,* not significant.

sion of Nanog in NIH-3T3 cells and did not mediate significant cell proliferation (supplemental Fig. S13).

Nanog is necessary for angiogenic activities in ECs

To address the ability of NP12 to stimulate angiogenesis, we performed knockdown followed by rescue experiments in relation to EC proliferation and branching point structure formations in 2D-Matrigel. To knock down *Nanog*, we used two distinct *Nanog* shRNAs shown as *Nanog*-shRNA1 and *Nanog*-shRNA2. Control and *Nanog* knockdown ECs were treated with 60 nmol/liter NP12 overnight as shown in Fig. 7*a*, and thereafter, cell lysates were subjected to WB analyses (Fig. 7*b*). As expected, NP12 increased the expression of Nanog in these cells, whereas both *Nanog*-shRNA1 and *Nanog*-shRNA2 knocked down the *Nanog* gene effectively (Fig. 7*b*). To address specificities of two *Nanog* shRNAs, we also carried out re-expression of HA-tagged *Nanog* cDNA into Nanog-depleted cells (Fig. 7*b*). In parallel, these cells were subjected to anti-BrdU antibody staining as a measure of cell proliferation (Fig. 7, *c* and *d*). ECs receiving NP12 showed a significant increase in proliferation; conversely, *Nanog* knockdown decreased proliferation of these cells (Fig. 7, *c* and *d*). Importantly, following *Nanog* knockdown, the proliferation of ECs that received NP12 was significantly reduced compared with control groups (Fig. 7, *c* and *d*). Next, we also subjected these cells to 2D-Matrigel assay (see under "Materials and methods"). As expected, NP12 increased branching point structures significantly, whereas Nanog knockdown decreased angiogenic activities of these cells (Fig. 7, *e* and *f*). Re-expression of Nanog cDNA into Nanog-depleted cells restored, in part, the effect of loss of Nanog in these cells (Fig. 7, *e* and *f*). These results indicate the ability of NP12 to mediate angiogenic activities of ECs through Nanog.

Discussion

Here, we addressed whether NP12 can be used for limiting the extent of adverse myocardial remodeling seen after AMI. Accordingly, we showed that a nanomolar concentration of NP12: 1) increased phosphorylation of GSK-3β(Ser-9) and stabilized β-catenin; 2) prevented adverse myocardial remodeling in mice that previously experienced an AMI; and 3) mediated angiogenesis, thereby reestablishing blood flow to the infarcted zone partially through the activities of Nanog.

NP12 has been described as an allosteric inhibitor of GSK-3β (21). Importantly, NP12 provided a neuroprotective benefit and showed no toxic effects in humans (22–25). Hypoxia, myocardial infarction, or obstruction of coronary arteries mediates

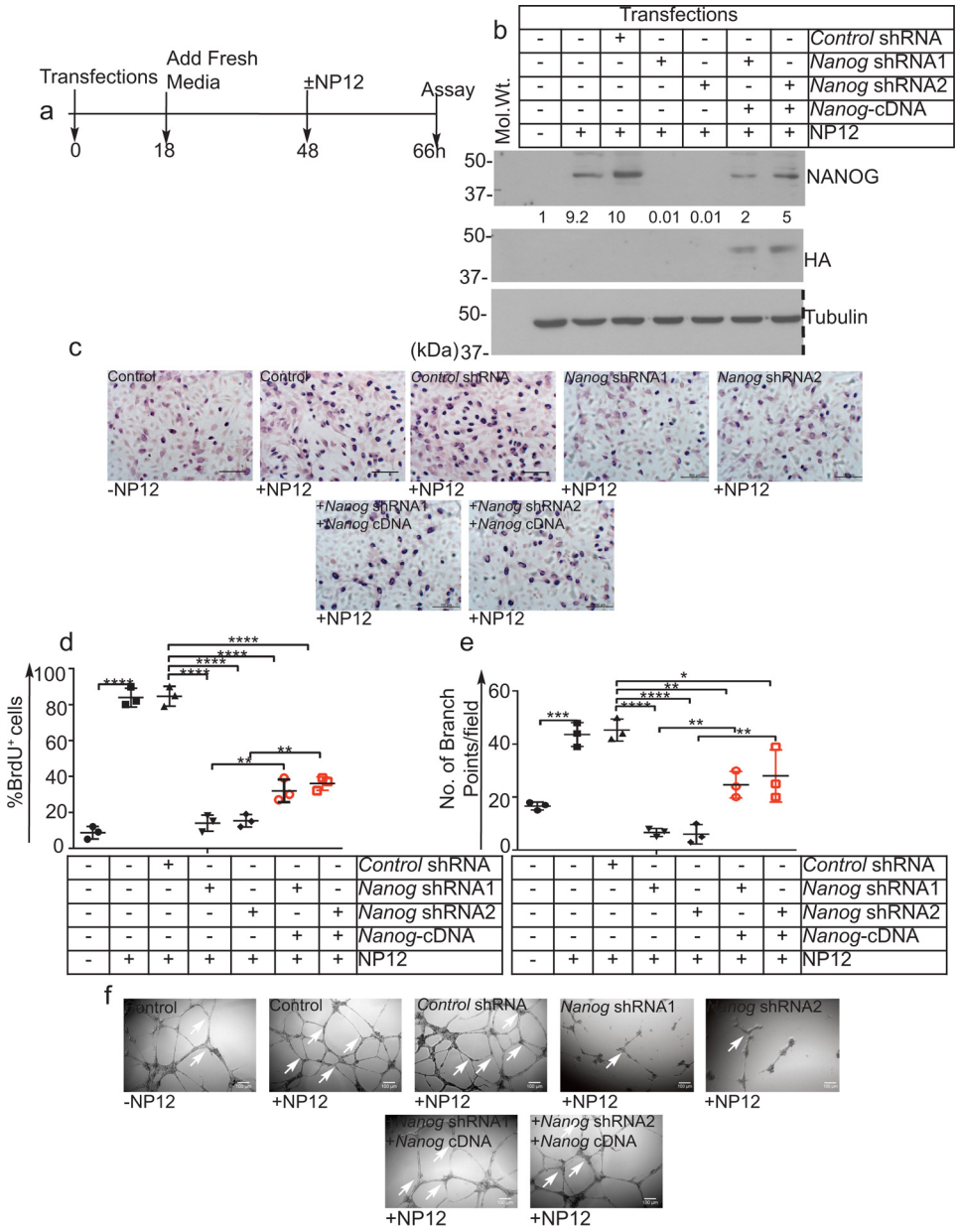

Figure 7. Nanog knockdown impairs NP12-mediated angiogenic activities of ECs. *a,* timeline of transfections (knockdown), followed by BrdU incorporation and 2D Matrigel assay. *b,* efficiency of *Nanog* knockdown using two distinct shRNA constructs followed by re-expression of HA-tagged *Nanog* cDNAs was analyzed by WB. The *numbers below* the panels indicate fold intensities. *Dotted line* indicates the position where nitrocellulose membrane was cut. *c,* representative images of $BrdU^+$ cells. *d,* quantification of $BrdU^+$ incorporation. *e,* quantification of branching point structures per field of view. *f,* representative images of branch point structures (*white arrows*) in control and *Nanog* knockdown and *Nanog* cDNA ECs receiving NP12. *Error bars* represent ± S.D., obtained from three independent experiments ($n = 3$), and each experiment was performed with two technical replicates; thereafter, data were subjected to ANOVA followed by Tukey's test. *, $p < 0.05$; **, $p < 0.01$; ***, $p < 0.001$; ****, $p < 0.0001$ *versus* indicated groups. *Scale bars* are as shown.

expression of VEGF. VEGF signaling is required for angiogenic and survival activities of ECs; and for this reason, we did not address the role of VEGF in this study. Wnt signaling plays a complex role in the emergence of ECs and cardiovascular disease processes (10, 35). At basal state, the GSK-3 proteins act as active kinase but are inhibited in response to several pathophysiological events, including AMI. However, the regulation of myocardial repair in the aftermath of AMI likely involves several different competing signaling pathways, including the inhibition of GSK-3 and cooperation of several cell types. Nevertheless, here we showed that NP12-mediated Nanog expression regulated angiogenic phenotypes of ECs in mice that experienced AMI. AMI due to LAD ligation results in damage of myocardial tissue, leading to collagen deposition and fibrosis. Our morphometric and quantification analyses showed reduced fibrotic scarring in mice receiving NP12, indicating the ability of NP12 to prevent adverse myocardial remodeling. ECG evaluation of the LV showed improvements in both EF% and FS%. These findings suggest that in uninjured mice, NP12 alone has no effect. Our data highlighted the ability of NP12 to limit the extent of unwanted myocardial remodeling.

The decrease in the extent of pathological myocardial remodeling in the aftermath of AMI likely involves complex interplay between different cell types and signaling pathways

(31–34). However, ECs are expected to play a critical role in the rescue process. Importantly, in adults, the loss of ECs impedes revascularization and worsens tissue damage; therefore, preventing EC death and increasing proliferation increase productive revascularization. Because we observed increased revascularization in the NP12-treated infarcted zone, we determined the effects of NP12 treatment on EC proliferation and survival; indeed, ECs treated with NP12 not only increased proliferation but also enhanced survival. The additive effect of NP12 treatment was secondary to VEGF, because VEGF is a well-known EC-specific mitogen and survival factor. Consistent with these observations, NP12 significantly increased cell proliferation, but decreased apoptosis, indicating the ability of NP12 administration to provide protective benefit.

EC migration is a pre-requisite process in neovessel formation; accordingly, we showed that NP12 treatment not only increased proliferation and viability but also enhanced EC migration *in vitro*. Can NP12 mediate migration *in vivo*? To address this, we analyzed microvessel growth from mouse aortic rings, an *ex vivo* correlate of angiogenesis. In this assay, NP12 mediated stable and robust sprouting of aortic rings and provided evidence that NP12 administration can enhance angiogenic activities of intact ECs. Based upon these findings, we predict that NP12 induces migration of ECs *in vivo*, after injury/wound.

These findings provided us with the impetus to delineate the molecular targets of GSK-3β inhibition in ECs. The Wnt pathway is initiated by nuclear translocation of β-catenin, which then forms a complex with the TCF4 family of transcription factors and leads to active transcription of Wnt target genes. In transfection experiments, NP12 significantly increased luciferase reporter activity, which was mediated by the nuclear translocation of β-catenin. This translocation is a key event, which increases cyclin-D1-mediated cell proliferation after NP12 treatment. Therefore, our data showed the ability of NP12 to mediate activation of canonical Wnt signaling in ECs. This is an important finding, as EC proliferation crucially regulates wound repair and re-establishes the supply of blood to the injured tissues, *e.g.* seen after AMI in our model.

Mechanistically, NP12 administration stabilized β-catenin expression and induced the expression of genes and proteins that regulate wound healing and re-establish blood supply. Although this result could indicate pan-cellular expression of β-catenin *in vivo*, it was evident that NP12 amplified the expression of Wnt target genes post-AMI. Therefore, it was not surprising that we found an increased p-GSK-3β(Ser-9) in response to NP12 treatment. Because non-ATP allosteric inhibitors are highly selective and effective at low dose, this could provide an explanation for the robust stabilization of β-catenin within a short period of time, as compared with that observed following Wnt3a stimulation. These interpretations are not only relevant to *in vitro* findings but are also confirmed by *in situ* labeling experiments of β-catenin and Nanog in conjunction with $CD31^+$ vascular structures. It is clear that human heart that experienced AMI becomes irreversible within an hour; however, reestablishment of flow of blood even after permanent coronary occlusion is a clinically desirable goal. Thus, we propose that N12 or allosteric inhibition of GSK-3β in the aftermath of AMI should provide therapeutic benefit.

Cell proliferation and tube formation represent two key hallmarks of the cellular behavior of ECs. Using loss-of-function and gain-of-function approaches, we addressed the specificity of Nanog in reestablishing blood supply in response to NP12. In these experiments, NP12 induced Nanog expression, thereby mediating cell proliferation. Thus, proliferative activities seen in the above experiments are likely Nanog-specific, as Nanog depletion inhibited angiogenic phenotypes of these cells. We propose that one of the key functions of NP12 is to stimulate EC proliferation and tube formation. Thus, proliferative and tube-forming activities of ECs are not only required for restoration of the structural integrity of the heart but also re-establish blood supply and decrease adverse remodeling after injury.

Data presented indicate the ability of a novel allosteric inhibitor of GSK-3β-mediated revascularization in the aftermath of AMI-induced injury and improved cardiac function by reducing fibrosis and apoptosis. In this study, we administered NP12 after the release of ligation, leading to a reduction in the infarct size after AMI. However, we propose that administration of NP12 secondary to increased expression of VEGF acts in synergy to mediate increased migration and proliferation, thereby reestablishing the flow of blood and reducing adverse myocardial remodeling. One could surmise that the NP12 treatment likely induced Wnt signaling not only in ECs but also in non-EC population such as either cardiomyocytes or fibroblast cells as well. However, we did not detect expression of Nanog in murine fibroblast cells *in vitro*. It will be interesting to study the effect of NP12 on cardiomyocytes; however, this is beyond the scope of this study and will require detailed analysis. Nevertheless, our results show that inhibition of GSK-3β thereafter increased expression of β-catenin and Nanog in ECs after AMI and together represent an endogenous repair mechanism, and the magnitude of Nanog and VEGFR2 expression can further be increased by NP12. Nanog likely activates several other genes, and VEGF/VEGFR2 signaling is critical for cardiovascular phenotypes and their survival. Reestablishing blood supply has the potential to protect myocardial structure and decrease fibrosis after AMI, and these processes are also necessary to prevent impending AMI through the regulation of cardiomyocyte hypertrophy and contractility. Together, our studies provide proof-of-principle of the potential of allosteric inhibition of GSK-3β for activating a repair machinery to improve flow of blood supply and to prevent adverse remodeling after AMI.

Materials and methods

Antibodies and reagents

NP12 (SML0339), human thrombin (T4393), and fibrinogen (F4883) were purchased from Sigma, and a 50 mmol/liter stock of NP12 was prepared in dimethyl sulfoxide (Sigma) and stored at −20 °C. A working concentration of 60 nmol/liter NP12 was used for all experiments. Rabbit anti-Nanog (A300-397A) was purchased from Bethyl (Montgomery, TX). Rabbit anti-VEGFR2 (C-1158), rabbit anti-cyclin-D1 (mAb catalog no. 2978), rabbit anti-phospho-GSK-3β (mAb catalog no. 9322), rabbit anti-

GSK-3β (mAb catalog no. 9315), rabbit anti-Akt (mAb catalog no. 9272), rabbit anti-p-Akt (mAb catalog no. 9271), and rabbit anti-TCF4 (mAb catalog no. 2569) were purchased from Cell Signaling Technologies (Danvers, MA). Mouse anti-Nanog (J-29), mouse anti-β-catenin (E5), mouse anti-glyceraldehyde-3-phosphate dehydrogenase (GAPDH, 4G5), and mouse anti-VE-cadherin (SC9989) were purchased from Santa Cruz Biotechnology (Dallas, TX). Rabbit anti-HA (AP1012a) was purchased from Abgent (San Diego). Secondary antibodies goat anti-mouse immunoglobulin G (IgG)–horseradish peroxidase (HRP) and donkey anti-rabbit IgG–HRP were purchased from Bio-Rad. Donkey anti-rabbit Alexa Fluor-594 and donkey anti-mouse Alexa Fluor-488 were purchased from Invitrogen. Human recombinant Wnt3a (5036-WN) was purchased from R&D Systems (Minneapolis, MN).

Animal experiments and echocardiography (ECG)

All animal experiments described in this study were performed in accordance with the National Institute of Health Committee (IACUC) at the University of Illinois at Chicago. Male and female C57BL/6N mice ($n = 6$ per group) between the ages of 8 and 10 weeks were purchased from The Jackson Laboratory (Bar Harbor, ME) and housed at the UIC vivarium. All procedures were performed at the Center for Cardiovascular Physiology core facility at UIC. To model AMI in the myocardium, mice were subjected to transient ligation (20 min) of the LAD coronary artery as described previously with minor modifications (26–28). Prior to coronary artery ligation, mice were administered intraperitoneal injection of etomidate (10 mg/kg) anesthesia. Thereafter, an 8-0 Prolene suture (Ethicon Inc., Sommerville, NJ) was used to slipknot and temporarily ligate the LAD coronary artery. After 20 min of ligation, the slipknot was released. ECG was measured prior to LAD ligation (pre-AMI) and post-ligation (post-AMI) at days 7 and 14 using Vevo-2100 (VisualSonics, Toronto, Ontario, Canada). To maintain the anesthesia during the surgery procedure, 2% isoflurane was delivered using a face mask. As our goal was to administer NP12 directly into the myocardium, accordingly, a working concentration of NP12 was prepared in sterile 1× PBS (vehicle) to prevent toxicity to myocardial tissue. A total of 12 μmol/liter NP12 were administered intramyocardially at three sites near the infarcted zone after release of ligation. The control group received 10 μl of PBS at the corresponding sites. Prior to surgery, subcutaneous injection of Buprenex SR-LAB (1 mg/kg body weight) was given, and mice were monitored every day for 4 days following surgery; thereafter, every alternate 2 days until post hoc analyses. For pilot experiments, sham-operated mice underwent the same procedure without ligation of the artery and received PBS and NP12. None of the mice displayed major bleeding or signs of infections during the post-operative monitoring phase until days 7 and 14. At days 7 and 14, mice were euthanized, and hearts were removed and washed with PBS. Tissues were paraffin-embedded for immunohistochemistry or snap-frozen in dry ice/ethanol bath for RNA and protein studies. Isolation of $CD31^+$ ECs has been previously described by us (38).

Morphometric analyses

For immunohistochemistry, hearts were excised and cut into three equal regions. The mid-region was paraffin-embedded and cut into 5-μm sections. ECs were labeled using mouse anti-CD31 (JC70A, Dako) and mouse anti-annexin-V (Sc-32321) and rabbit anti-PECAM1/CD31 (Sc-1506) were purchased from Santa Cruz Biotechnology (Dallas, TX); mouse anti-Nanog (MABD24) and rabbit anti-von Willebrand factor (AB7356) were purchased from Millipore (Billerica, MA); mouse anti-α-smooth muscle actin (αSMA; clone 1A40) was from Sigma, mouse anti-Ki67 (B56-RUO) and rabbit anti-β-catenin (ABE208) were from Millipore and were followed by incubation with secondary anti-rabbit 594 (Invitrogen) and anti-mouse 488 (Invitrogen). Fluorescent images (×63) were captured using a Zeiss LSM 880 confocal microscope (Carl Zeiss AG, Oberkochen, Germany) and analyzed with Zen 2011 software (Carl Zeiss AG). Masson's trichrome staining and TUNEL staining were performed at the UIC histology core facility. Five fields from infarcted and control heart sections were evaluated with an Olympus BX51/IX70 fluorescence microscope (Olympus, Tokyo, Japan). Morphometric analyses of the hearts were assessed using ImageJ software (National Institutes Health, Bethesda).

Cell culture and Western blot analysis

HUVECs, HPAECs, and human lung microvascular ECs were purchased from Lonza (Allendale, NJ) and cultured up to 3–4 passages as described previously (19, 20, 37, 40). HSaVECs were obtained from PromoCell (Heidelberg, Germany) and cultured as described previously (19, 20). Cells were solubilized in radioimmunoprecipitation assay (RIPA) protein extraction buffer containing protease inhibitors. Protein concentrations were determined using Pierce 660-nm reagent (Thermo Fisher Scientific, Waltham, MA), resolved by SDS-PAGE, and proteins were transferred onto nitrocellulose membrane. Primary antibodies (2.0 μg/ml) were prepared in 1× TBS, pH 7.4, containing 3% BSA. All other WB procedures have been described previously (37, 39, 40).

Immunostaining and microscopy

This method has been previously described (19, 20, 40). In brief, monolayer ECs were left untreated (control) or treated with NP12 for 6 h. Nuclear localization of β-catenin and TCF4 was captured by high-resolution (×40 and ×63) confocal microscopy (Carl Zeiss AG) at room temperature, and multiple images were analyzed using Zen 2011 software (Carl Zeiss AG). Raw images were saved as czi, TIFF, or EPS documents, and all figures were assembled using QuarkExpress 2016 and Adobe Photoshop 2017. For quantification, we used ImageJ.

Transfection experiments and reporter assays

shRNA-mediated *Nanog* knockdown and transfection methods have been previously described (37, 40). Control (T30015) and *Nanog* shRNA constructs (catalog no. TF303039) were purchased from Origene (Rockville, MD). For knockdown experiments, high-titer lentivirus particles generated from the construct FI312151 (*Nanog*-shRNA1, AAACAGGTGAAGACCTGGTT-

Table 1
Gene-specific oligonucleotide sequences used for qRT-PCR experiments
F is forward; R is reverse.

	Name	Species	Sequence (5′–3′)	Accession no.
1	*Nanog*	Human	(F) 5′-TTAGTAGAGACGGGGTTTCACTG-3′ (R) 5′-GTGGATCACAAGGTCAGGAGAT-3′	NM_024865.3
2	*Cyclin-D1*	Human	(F) 5′-CCAACAACTTCCTGTCCTACTACC-3′ (R) 5′-GGTCACACTTGATCACTCTGGA-3′	BC000076.2
3	*VEGFR2*	Human	(F) 5′-GTGTGGTGTCAAAGTTTCAGGAAG-3′ (R) 5′-GGTTTACTGGAGTAGAGGCCAAAT-3′	NM_002253.2
4	*18S* rRNA	consensus	(F) 5′-GGAGGTTCGAAGACGATCAGA-3′ (R) 5′-GCATCGTTTATGGTCGGAACT-3′	NR_003286.2
5	*Nanog*	Mouse	(F) 5′-ATGTTTAAGGTCGGGCTGTAGA-3′ (R) 5′-GAGTGACAGGACATTCGAACAA-3′	NC_000072.6
6	*Cyclin-D1*	Mouse	(F) 5′-CGTACCCTGACACCAATCT-3′ (R) 5′-ATCTCCTTCTGCACGCACTT-3′	NC_000073.6
7	*VEGFR2*	Mouse	(F) 5′-TAGCTCATGCCAGTACCTGAGA-3′ (R) 5′-AAGGAAGTAGAATCCCCTCGAG-3′	XM_006496487.3
8	*Ki-67*	Mouse	(F) 5′-AGGCAGCTAAGGACACATAAGG-3′ (R) 5′-CGTTCCTCTAGACCTCAAGCAT-3′	XM_006507411.2

CCAGAACCA) and construct FI312152 (*Nanog*-shRNA2, CAGAACATCCAGTCCTGGAGCAACCACTC) were used to infect ECs. For rescue experiments, we transfected hemagglutinin (HA)-tagged *Nanog* cDNA (lot: 102036S-2/T98134, GenScript (Piscataway, NJ) into *Nanog*-depleted ECs. To monitor the activation of NP12-mediated Wnt signaling, ECs and HEK293T cells were transiently co-transfected with super 8×TOPFlash plasmids containing eight copies of TCF4/LEF-1-binding sites (gift of Randall T. Moon) and a β-galactosidase plasmid at a 3:1 ratio. After overnight transfection, cells were serum-starved for 3 h, followed by the addition of Wnt3a (50 ng/ml) and NP12 (60 nmol/liter) into the basal media and incubated for an additional 3 h. Cell lysates were prepared according to the manufacturer's instructions (Promega, Madison, WI). Luciferase activity as a function of the activation of the TCF-4/LEF-1 promoter was measured using a standard luminometer (Berthold Technologies, Oak Ridge, TN), and luciferase activity was normalized to β-galactosidase enzyme activity as described previously (19, 20). Experiments were performed in triplicates and repeated at least three times.

Gene expression, 5′-bromo-2′-deoxyuridine, and apoptosis assays

Methods for mRNA preparation and qRT-PCR have been previously described (19, 20). Gene-specific primers (Table 1) were synthesized by IDT DNA (Coralville, IA). To monitor cell proliferation, BrdU assays were performed as described previously (19), and an Axiovert 40C microscope (Carl Zeiss AG) was used to record all digital pictures. For quantification, ImageJ software was used. To assess cell death, ECs were serum-starved in minimal basal media containing 1× insulin/transferrin selenium (41400-045; Life Technologies, Inc.). Cells receiving either VEGF, NP12, or both were incubated overnight. The percentage of cell death was quantified using an annexin-V apoptosis detection kit APC (88-8007-72; eBioscience, San Diego) as described previously (19, 20). Cells were sorted using a Beckman-Coulter flow cytometer (Brea, CA). Experiments were performed more than three times.

Cell migration experiments

These methods have been previously described by us (19, 20). In brief, a scratch was introduced in monolayer ECs using a sterile 200-μl pipette tip. Detached cells were removed by a PBS wash, and fresh media containing vehicle alone (control) or 60 nmol/liter NP12 was added. Images of wound closure were taken at 0, 3, and 6 h using an Axiovert 40C microscope (×10; Carl Zeiss AG). The percentage of wound closure was quantified using ImageJ. For the chemotactic cell-migration assay, Boyden-chamber inserts containing 5,000 cells in the upper chamber were placed in 24-well culture plates; and EC media (vehicle alone) or with NP12 was placed in the lower wells. After 6 h, cells that had migrated across the membrane were fixed and stained with crystal violet. Images were captured as described previously, and the percentages of migrated cells in response to NP12 *versus* control were quantified using ImageJ.

Aortic ring and 2D Matrigel assays

The aortic ring and 2D Matrigel assays have been previously described (19, 37). Briefly, the thoracic aortas from to 2-week-old male BALB/c mice were excised, and ~1-mm aortic rings were embedded in 80 μl of fibrin gel matrix supplemented with EndoGro media (Millipore) containing vehicle alone or with 60 nmol/liter NP12. Images of the aortic explants were captured at days 0 and 4 using a Zeiss Axiovert 40C microscope (Carl Zeiss AG). The aortic ring sprouts were quantified using ImageJ. For quantification, at least 10 different microscopic fields were selected randomly from one aortic ring.

Statistical analyses

For statistical analyses, GraphPad Prism 6.0 (GraphPad Software, La Jolla, CA) was used. An unpaired Student's *t* test was used for comparisons between two groups, and analysis of variance (ANOVA) followed by Tukey's or Sidak's or Dunnett's test for multiple comparisons. All data points represent mean ± S.D. The number of experiments or the number of animals represents biological replicates. A $p < 0.05$ was considered significant.

Author contributions—J. B. designed oligonucleotides, characterized NP12-mediated activation of Wnt pathway, carried out transfections and reporter assays, performed Western blottings, expression analyses, post-surgical monitoring of mice, immunohistochemical and morphometric analysis, collected data, assembled figures and images, and prepared the manuscript. R. H. performed immunostaining, microscopy, q-RT-PCR, assembled staining images, and post-surgical monitoring of mice. J. Z. did immunostaining, microscopy, and q-RT-PCR. Physiology core conducted animal surgery, coronary artery ligation, and EGC. S. C. and V. M. did immunohistochemistry and data analysis. K. K. W. conceived the hypothesis, designed experiments, interpreted the data, and prepared and finalized the manuscript.

Acknowledgments—We acknowledge the RRC Core Imaging Facility, Flow Cytometry Service, Cardiovascular Physiology Core, Research Histology, and Tissue Imaging Cores of the University of Illinois at Chicago.

References

1. Marijianowski, M. M., Teeling, P., and Becker, A. E. (1997) Remodeling after myocardial infarction in humans is not associated with interstitial fibrosis of noninfarcted myocardium. *J. Am. Coll. Cardiol.* **30,** 76–82
2. van den Borne, S. W., Diez, J., Blankesteijn, W. M., Verjans, J., Hofstra, L., and Narula, J. (2010) Myocardial remodeling after infarction: the role of myofibroblasts. *Nat. Rev. Cardiol.* **7,** 30–37
3. Thygesen, K., Alpert, J. S., Jaffe, A. S., Simoons, M. L., Chaitman, B. R., White, H. D., Task Force for the Universal Definition of Myocardial Infarction (2012) Third universal definition of myocardial infarction. *Nat. Rev. Cardiol.* **9,** 620–633
4. Anderson, J. L., and Morrow, D. A. (2017) Acute myocardial infarction. *N. Engl. J. Med.* **376,** 2053–2064
5. Zhang, R., Hess, D. T., Reynolds, J. D., and Stamler, J. S. (2016) Hemoglobin *S*-nitrosylation plays an essential role in cardioprotection. *J. Clin. Invest.* **126,** 4654–4658
6. Cambier, L., de Couto, G., Ibrahim, A., Echavez, A. K., Valle, J., Liu, W., Kreke, M., Smith, R. R., Marbán, L., and Marbán, E. (2017) Y RNA fragment in extracellular vesicles confers cardioprotection via modulation of IL-10 expression and secretion. *EMBO Mol. Med.* **9,** 337–352
7. Hausenloy, D. J., Garcia-Dorado, D., Bøtker, H. E., Davidson, S. M., Downey, J., Engel, F. B., Jennings, R., Lecour, S., Leor, J., Madonna, R., Ovize, M., Perrino, C., Prunier, F., Schulz, R., Sluijter, J. P. G., *et al.* (2017) Novel targets and future strategies for acute cardioprotection: Position Paper of the European Society of Cardiology Working Group on Cellular Biology of the Heart. *Cardiovasc. Res.* **113,** 564–585
8. Juhaszova, M., Zorov, D. B., Kim, S.-H., Pepe, S., Fu, Q., Fishbein, K. W., Ziman, B. D., Wang, S., Ytrehus, K., Antos, C. L., Olson, E. N., and Sollott, S. J. (2004) Glycogen synthase kinase-3β mediates convergence of protection signaling to inhibit the mitochondrial permeability transition pore. *J. Clin. Invest.* **113,** 1535–1549
9. Zhai, P., Sciarretta, S., Galeotti, J., Volpe, M., and Sadoshima, J. (2011) Differential roles of GSK-3β during myocardial ischemia and ischemia/reperfusion. *Circ. Res.* **109,** 502–511
10. Lal, H., Zhou, J., Ahmad, F., Zaka, R., Vagnozzi, R. J., Decaul, M., Woodgett, J., Gao, E., and Force, T. (2012) Glycogen synthase kinase-3α limits ischemic injury, cardiac rupture, post-myocardial infarction remodeling and death. *Circulation* **125,** 65–75
11. Duan, J., Gherghe, C., Liu, D., Hamlett, E., Srikantha, L., Rodgers, L., Regan, J. N., Rojas, M., Willis, M., Leask, A., Majesky, M., and Deb, A. (2012) Wnt1/βcatenin injury response activates the epicardium and cardiac fibroblasts to promote cardiac repair. *EMBO J.* **31,** 429–442
12. Lal, H., Ahmad, F., Woodgett, J., and Force, T. (2015) The GSK-3 family as therapeutic target for myocardial diseases. *Circ. Res.* **116,** 138–149
13. Terashima, Y., Sato, T., Yano, T., Maas, O., Itoh, T., Miki, T., Tanno, M., Kuno, A., Shimamoto, K., and Miura, T. (2010) Roles of phospho-GSK-3β in myocardial protection afforded by activation of the mitochondrial K ATP channel. *J. Mol. Cell. Cardiol.* **49,** 762–770
14. Miura, T., and Tanno, M. (2010) Mitochondria and GSK-3β in cardioprotection against ischemia/reperfusion injury. *Cardiovasc. Drugs Ther.* **24,** 255–263
15. Deb, A. (2014) Cell-cell interaction in the heart via Wnt/β-catenin pathway after cardiac injury. *Cardiovasc. Res.* **102,** 214–223
16. Clevers, H., Loh, K. M., and Nusse, R. (2014) Stem cell signaling. An integral program for tissue renewal and regeneration: Wnt signaling and stem cell control. *Science* **346,** 1248012
17. Loh, K. M., van Amerongen, R., and Nusse, R. (2016) Generating cellular diversity and spatial form: Wnt signaling and the evolution of multicellular animals. *Dev. Cell* **38,** 643–655
18. Patel, P., and Woodgett, J. R. (2017) Glycogen synthase kinase 3: a kinase for all pathways? *Curr. Top. Dev. Biol.* **123,** 277–302
19. Kohler, E. E., Cowan, C. E., Chatterjee, I., Malik, A. B., and Wary, K. K. (2011) NANOG induction of fetal liver kinase-1 (FLK1) transcription regulates endothelial cell proliferation and angiogenesis. *Blood* **117,** 1761–1769
20. Kohler, E. E., Baruah, J., Urao, N., Ushio-Fukai, M., Fukai, T., Chatterjee, I., and Wary, K. K. (2014) Low-dose 6-bromoindirubin-3′-oxime induces partial dedifferentiation of endothelial cells to promote increased neovascularization. *Stem Cells* **32,** 1538–1552
21. Domínguez, J. M., Fuertes, A., Orozco, L., del Monte-Millán, M., Delgado, E., and Medina, M. (2012) Evidence for irreversible inhibition of glycogen synthase kinase-3β by tideglusib. *J. Biol. Chem.* **287,** 893–904
22. Lovestone, S., Boada, M., Dubois, B., Hüll, M., Rinne, J. O., Huppertz, H.-J., Calero, M., Andrés, M. V., Gómez-Carrillo, B., León, T., del Ser, T., and ARGO investigators. (2015) A phase II trial of tideglusib in Alzheimer's disease. *J. Alzheimers Dis.* **45,** 75–88
23. Höglinger, G. U., Huppertz, H.-J., Wagenpfeil, S., Andrés, M. V., Belloch, V., León, T., Del Ser, T., and TAUROS MRI Investigators. (2014) Tideglusib reduces progression of brain atrophy in progressive supranuclear palsy in a randomized trial. *Mov. Disord.* **29,** 479–487
24. Tolosa, E., Litvan, I., Höglinger, G. U., Burn, D., Lees, A., Andrés, M. V., Gómez-Carrillo, B., León, T., Del Ser, T., and TAUROS Investigators. (2014) A phase 2 trial of the GSK-3 inhibitor tideglusib in progressive supranuclear palsy. *Mov. Disord.* **29,** 470–478
25. del Ser, T., Steinwachs, K. C., Gertz, H. J., Andrés, M. V., Gómez-Carrillo, B., Medina, M., Vericat, J. A., Redondo, P., Fleet, D., and León, T. (2013) Treatment of Alzheimer's disease with the GSK-3 inhibitor tideglusib: a pilot study. *J. Alzheimers Dis.* **33,** 205–215
26. Gaffin, R. D., Peña, J. R., Alves, M. S., Dias, F. A., Chowdhury, S. A., Heinrich, L. S., Goldspink, P. H., Kranias, E. G., Wieczorek, D. F., and Wolska, B. M. (2011) Long-term rescue of a familial hypertrophic cardiomyopathy caused by a mutation in the thin filament protein, tropomyosin, via modulation of a calcium cycling protein. *J. Mol. Cell. Cardiol.* **51,** 812–820
27. Preda, M. B., and Burlacu, A. (2010) Electrocardiography as a tool for validating myocardial ischemia-reperfusion procedures in mice. *Comp. Med.* **60,** 443–447
28. Scofield, S. L., and Singh, K. (2016) Confirmation of myocardial ischemia and reperfusion injury in mice using surface pad electrocardiography. *J. Vis. Exp. 2016*
29. Kornowski, R., Fuchs, S., Leon, M. B., and Epstein, S. E. (2000) Delivery strategies to achieve therapeutic myocardial angiogenesis. *Circulation* **101,** 454–458
30. Zhao, J., Wang, F., Zhang, Y., Jiao, L., Lau, W. B., Wang, L., Liu, B., Gao, E., Koch, W. J., Ma, X.-L., and Wang, Y. (2013) Sevoflurane preconditioning attenuates myocardial ischemia/reperfusion injury via caveolin-3-dependent cyclooxygenase-2 inhibition. *Circulation* **128,** S121–S129
31. Pagel, P. S., Krolikowski, J. G., Neff, D. A., Weihrauch, D., Bienengraeber, M., Kersten, J. R., and Warltier, D. C. (2006) Inhibition of glycogen synthase kinase enhances isoflurane-induced protection against myocardial infarction during early reperfusion *in vivo*. *Anesth. Analg.* **102,** 1348–1354
32. van Berlo, J. H., and Molkentin, J. D. (2014) An emerging consensus on cardiac regeneration. *Nat. Med.* **20,** 1386–1393
33. Fan, D., Takawale, A., Shen, M., Wang, W., Wang, X., Basu, R., Oudit, G. Y., and Kassiri, Z. (2015) Cardiomyocyte A disintegrin and metallopro-

teinase 17 (ADAM17) is essential in post-myocardial infarction repair by regulating angiogenesis. *Circ. Heart Fail.* **8,** 970–979
34. Bonaventura, A., Montecucco, F., and Dallegri, F. (2016) Cellular recruitment in myocardial ischaemia/reperfusion injury. *Eur. J. Clin. Invest.* **46,** 590–601
35. Woulfe, K. C., Gao, E., Lal, H., Harris, D., Fan, Q., Vagnozzi, R., DeCaul, M., Shang, X., Patel, S., Woodgett, J. R., Force, T., and Zhou, J. (2010) Glycogen synthase kinase-3β regulates post-myocardial infarction remodeling and stress-induced cardiomyocyte proliferation *in vivo*. *Circ. Res.* **106,** 1635–1645
36. Cieslik, K. A., Trial, J., Crawford, J. R., Taffet, G. E., and Entman, M. L. (2014) Adverse fibrosis in the aging heart depends on signaling between myeloid and mesenchymal cells; role of inflammatory fibroblasts. *J. Mol. Cell. Cardiol.* **70,** 56–63
37. Usatyuk, P. V., Fu, P., Mohan, V., Epshtein, Y., Jacobson, J. R., Gomez-Cambronero, J., Wary, K. K., Bindokas, V., Dudek, S. M., Salgia, R., Garcia, J. G., and Natarajan, V. (2014) Role of c-Met/phosphatidylinositol 3-kinase (PI3k)/Akt signaling in hepatocyte growth factor (HGF)-mediated lamellipodia formation, reactive oxygen species (ROS) generation, and motility of lung endothelial cells. *J. Biol. Chem.* **289,** 13476–13491
38. Wary, K. K., Vogel, S. M., Garrean, S., Zhao, Y. D., and Malik, A. B. (2009) Requirement of α(4)β(1) and α(5)β(1) integrin expression in bone-marrow-derived progenitor cells in preventing endotoxin-induced lung vascular injury and edema in mice. *Stem Cells* **27,** 3112–3120
39. Humtsoe, J. O., Liu, M., Malik, A. B., and Wary, K. K. (2010) Lipid phosphate phosphatase 3 stabilization of β-catenin induces endothelial cell migration and formation of branching point structures. *Mol. Cell. Biol.* **30,** 1593–1606
40. Cowan, C. E., Kohler, E. E., Dugan, T. A., Mirza, M. K., Malik, A. B., and Wary, K. K. (2010) Kruppel-like factor-4 transcriptionally regulates VE-cadherin expression and endothelial barrier function. *Circ. Res.* **107,** 959–966

The allosteric glycogen synthase kinase-3 inhibitor NP12 limits myocardial remodeling and promotes angiogenesis in an acute myocardial infarction model

Jugajyoti Baruah, Ryan Hitzman, Jane Zhang, Suhnrita Chaudhuri, Victoria Mastej and Kishore K. Wary

J. Biol. Chem. 2017, 292:20785-20798.
doi: 10.1074/jbc.M117.814376 originally published online October 25, 2017